Trajectory Simulation for Air Traffic Management Employing a Multirotor Urban Air Mobility Aircraft Model

Gano B. Chatterji*
Crown Consulting Inc. at NASA Ames Research Center, Moffett Field, CA, 94035-1000

This paper describes a point-mass model of a multirotor electric vertical takeoff and landing aircraft designed to carry up to five passengers and a pilot. The model employs thrust, thrust vector angle and bank angle as controls, which are computed in part using the acceleration, heading-angle rate, and flight-path-angle rate generated by control systems in response to speed, heading angle, and flight-path angle commands. The equations of motion are integrated forward in time using the controls needed for following the desired vertical climb/descent and speed profiles, and horizontal path and cruise speed in the presence of wind to generate the flight trajectory.

I. Introduction

The motivation for developing an aircraft performance model of a multirotor Urban Air Mobility (UAM) aircraft is to enable generation of trajectories, which are needed for concept evaluation studies and in decision support tools. One of the challenges facing the future Air Traffic Management (ATM) system is integrating new entrants like UAM, Unmanned Aerial Systems (UAS), supersonic aircraft and space-launch vehicles in the U. S. National Airspace System (NAS) with legacy commercial subsonic and General Aviation (GA), while accommodating the business and operational objectives of all stakeholders. The ability to simulate UAM trajectories is essential because they will be used both by the flight operator and the ATM service provider for planning and control purposes. For example, the flight operator will use generated trajectories to determine route of flight, energy consumption, cruise speed, cruise altitude and time of arrival considering forecast winds aloft and alternative landing sites (airports and vertiports) that can be reached from locations along the route for creating flight-plan alternatives. The service provider will employ trajectories for separation assurance and traffic flow management. Separation assurance requires predicting conflicts, generating resolution advisories and evaluating them. Traffic flow management requires forecasting traffic demand at constrained resources—airspace and landing sites—and for determining flow control initiatives such as ground-hold, metering and scheduling needed for preventing the available capacity from being exceeded.

In the past several years, different designs have been proposed for electric vertical takeoff and landing (eVTOL) aircraft by the industry. Designs by Ehang (https://www.ehang.com/ehangaav/), Lilium (https://www.lilium.com/), Joby (https://www.jobyaviation.com/), Kitty Hawk (https://kittyhawk.aero/), Boeing-Aurora (https://www.aurora.aero/) and Airbus-Acubed (https://acubed.airbus.com/) have included rotary wing aircraft with multiple rotors, fixed-wing multi-engine tiltrotor, fixed-wing tiltrotor with rear push-propellers, fixed-wing aircraft with multiple lift fans (upward pointing fixed propellers) and rear push-propellers, and multi-engine tiltwing. This paper presents a model of the rotary wing aircraft with multiple rotors and employs it for trajectory synthesis.

A trajectory can be generated by driving the mathematical model of the aircraft dynamics with a control system to follow the desired path. The output of the feedback control system for eliminating the difference between the desired state and the estimated state of the aircraft is fed as input to the model of the aircraft dynamics for temporal evolution of the state and outputs. This approach is adequate for traffic simulation and prediction needed for ATM applications. The other related applications of interest to the aviation community are estimator and control system design for estimating the state and controlling the motion of the physical aircraft, respectively. Both these applications require a mathematical model of the aircraft dynamics. Several six-degree-of-freedom models with different levels of complexity that include both the rotational and translational dynamics of a quadrotor aircraft, and controllers for them, are available in Ref. 1 through 5. The control problem has been solved in several different ways. Reference 1 employs nonlinear programming to generate the trajectory that minimizes the total impulse while staying outside a geographical region and subjecting the observer to less than or equal to the specified sound pressure level. Reference 2 uses an adaptive backstepping procedure for horizontal and vertical path tracking and attitude control. Reference 3 uses

* Senior Scientist and Lead, Crown Consulting, Inc., MS 210-8, Associate Fellow.

piecewise Proportional-Integral (PI) control in the along-track direction and Proportional-Integral-Derivative (PID) control in the cross-track direction for path tracking, which generates attitude reference commands. The attitude control law using feedback linearization and acceleration feedback is then used to track the attitude reference commands to orient the vehicle's thrust for generating the acceleration needed for tracking the desired path. Reference 5 linearizes the dynamics and control about an operating point to develop a Linear-Quadratic-Regulator (LQR) for flight control.

The main difficulty with including rotational dynamics for trajectory generation, as in Refs. 1 through 5, is that the moment of inertia tensor needs to be known. With multirotor UAM still being designed and being developed, these data are unavailable. Furthermore, aircraft manufacturers are hesitant to share data they consider proprietary and not required for the operator to fly the aircraft. In addition, an attitude controller for trajectory generation for ATM applications is unnecessary because the angular rates and the resulting attitude are not observable from position data obtained from air traffic control radar systems or from position data determined onboard the aircraft and broadcast to the ground. Only six states—latitude, longitude, altitude, speed, heading and climb/descent rate—are observable from surveillance data; therefore, they are the ones employed for ATM decision support. For example, Time-Based Flow Management (TBFM), which is used for scheduling arrivals to major U. S. airports, uses a trajectory synthesis procedure based on a point-mass model that only considers the translational dynamics of the aircraft to predict estimated times of arrival at the metering locations (see Ref. 6). Systems for simulating air traffic such as NASA's Future ATM Concepts Evaluation Tool (FACET) (see Ref. 7), Airspace Concept Evaluation System (ACES) (see Ref. 8) and ATM-X Testbed use Eurocontrol's Base-of-Aircraft-Data (BADA) (see Ref. 9) aircraft performance model for generating the flight trajectory without considering rotational dynamics. Due to these reasons, this paper only models the translational dynamics of multirotor aircraft and derives the controls using the states and the state derivatives, where the state derivatives are obtained using Proportional and Proportional-Derivative (PD) controllers. The Proportional controller is used for tracking the airspeed and the PD controller is used for tracking the horizontal path. The vertical profile is specified. It is shown that this model driven by the non-linear controller developed in this paper can generate trajectories for UAM mission requirements outlined in Ref. 10.

The rest of the paper is organized as follows. Section II provides a brief description of a conceptual aircraft model described in Ref. 11. The equations of motion are discussed in Section III. Computation of control variables—thrust, thrust vector angle and bank angle—is provided in Section IV. Prescription of heading and flight-path angles for following horizontal and vertical paths in the presence of wind is examined in Section V. Section VI describes the trajectory generation process and presents results for a flight scenario. The paper is concluded in Section VII.

II. Multirotor Aircraft Model

Parameters needed for generating the trajectory using the aircraft performance model presented in this paper are obtained from the battery-powered electric quadcopter concept vehicle described in Ref. 11. To size and analyze the aircraft designs, Ref. 11 used the NASA Design and Analysis of Rotorcraft (NDARC) tool. The NDARC tool provides models for rotors and lifting surfaces, engines and motors, and energy storage and conversion for requirements and technology trades for aircraft design. The quadcopter concept vehicle employs motors, shafts and gearboxes to power the four rotors. The aircraft performance model in this paper does not consider power topology of the quadcopter for modeling the power consumption and thrust generation by individual rotors; the total thrust and power consumption are modeled. The quadcopter aircraft parameters are listed in Table 1.

Table 1. Quadcopter eVTOL conceptual model parameters.

Parameter	Value
Structural Mass (excluding the battery)	1,684 kg
Mass of Single Passenger	91 kg
Maximum Number of Occupants (includes the pilot)	6 persons
Battery Mass	710 kg
Maximum Mass (with six occupants)	2,940 kg
Useful Battery Capacity (80% Battery Capacity)	295,778 watt hours
Maximum Deliverable Power	501,110 watts
Drag Coefficient	1.1984 dimensionless
Reference Area	1 square meter

III. Equations of Motion

The motion of aircraft, modeled as a point-mass, is described by the following three equations (see Ref. 12):

$$\dot{\lambda} = \frac{1}{(R+h)} V_{gn} \tag{1}$$

$$\dot{\tau} = \frac{1}{(R+h)\cos\lambda} V_{ge} \tag{2}$$

and

$$\dot{h} = V_h \tag{3}$$

where λ is the latitude, τ is the longitude, h is the geometric altitude and R is the mean radius of the Earth. V_{gn} and V_{ge} are the north and east components of the ground-relative aircraft velocity. V_h is the ground-relative climb or descent rate depending on whether it is positive or negative. The horizontal velocity of the aircraft with respect to the ground is the resultant of the horizontal components of the airmass-relative aircraft velocity and the ground-relative wind velocity. This relationship is shown in Fig. 1, where V_g and W_s are the magnitudes of the horizontal components of the ground-relative aircraft velocity and the wind velocity, and V_s is the magnitude of the horizontal component of the airmass-relative aircraft velocity. χ_g is the heading angle of the ground-relative aircraft velocity with respect to the local north direction. χ and χ_w are the heading angles of the airmass-relative aircraft velocity and ground-relative wind velocity, respectively, also with respect to the local north direction. W_n, W_e and W_h are the north, east and up components of the ground-relative wind velocity vector.

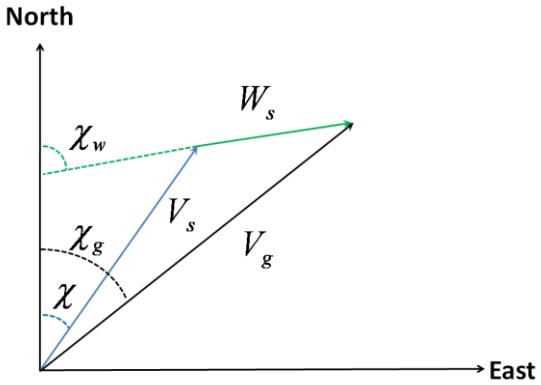

Figure 1. Velocity triangle.

The magnitude of the airmass-relative acceleration resulting from the thrust, drag, and gravitational forces on the multirotor aircraft modeled as a point-mass, defined in Fig. 2, is

$$\dot{V} = \frac{T\cos\delta - D}{m} - g\sin\gamma \tag{4}$$

where V is the airmass-relative speed (true airspeed), T is the thrust, D is the drag, δ is the thrust vector angle with respect to the airmass-relative velocity, m is the mass, g is the acceleration due to gravity and γ is the airmass-relative flight-path angle. Note that Eq. (4) assumes the wind acceleration to be zero. V_s is defined in terms of true airspeed and flight-path angle as

$$V_s = V\cos\gamma \tag{5}$$

The north, east and vertical components of the ground-relative aircraft velocity in terms of the true airspeed, flight-path angle, heading angle and wind terms are

$$V_{gn} = V\cos\gamma\cos\chi + W_n \tag{6}$$

$$V_{ge} = V\cos\gamma\sin\chi + W_e \tag{7}$$

and

$$V_h = V\sin\gamma + W_h \tag{8}$$

Using Eq. (6) and (7), groundspeed is obtained as

$$V_g = \sqrt{(V\cos\gamma\cos\chi + W_n)^2 + (V\cos\gamma\sin\chi + W_e)^2} \tag{9}$$

The state equations for airmass-relative heading angle and flight-path angle assuming wind acceleration to be zero can be written as follows:

$$\dot{\chi} = \frac{T\sin\delta\sin\mu}{mV\cos\gamma} \tag{10}$$

and

$$\dot{\gamma} = \frac{T\sin\delta\cos\mu}{mV} - \frac{g\cos\gamma}{V} \tag{11}$$

where μ is the airmass-relative bank angle. Equations (4), (10) and (11) are derived assuming flat Earth, constant gravitational acceleration and slowly changing mass. Mass is constant for battery-powered electric aircraft.

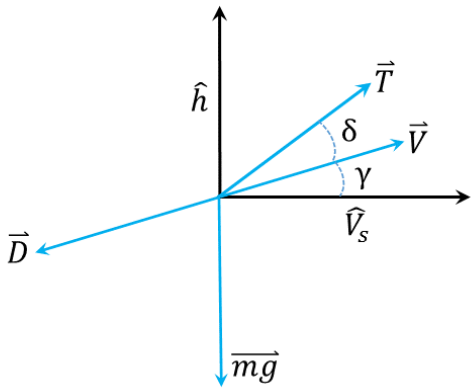

Figure 2. Forces on the multirotor aircraft.

To summarize, the state equations for the point-mass model of a multirotor aircraft are given by Eqs. (1) through (3), Eq. (4) and Eqs. (10) and (11), where the states are: λ, τ, h, V, χ and γ. The controls are: T, δ and μ, which can be determined as shown in the next section.

IV. Control Computation

Let the commanded airspeed, heading angle and flight-path angle be denoted by V_c, χ_c and γ_c, respectively. Let the commanded thrust, thrust vector angle and the bank angle be denoted by T_c, δ_c and μ_c, respectively. Based on the relationships in Eqs. (4), (10) and (11), the following equations can be written for computing the control variables.

$$T_c\cos\delta_c = m\dot{V}_c + D + mg\sin\gamma \tag{12}$$

$$T_c\sin\delta_c\sin\mu_c = mV\dot{\chi}_c\cos\gamma \tag{13}$$

and

$$T_c\sin\delta_c\cos\mu_c = mV\dot{\gamma}_c + mg\cos\gamma \tag{14}$$

Given that three equations are available for three unknowns, the unknowns can be determined as follows. Dividing Eq. (13) by Eq. (14), the commanded bank angle can be determined as

$$\mu_c = \tan^{-1}\left(\frac{V\dot{\chi}_c \cos\gamma}{V\dot{\gamma}_c + g\cos\gamma}\right) \tag{15}$$

Squaring and adding Eq. (13) and (14), taking the square root and dividing by Eq. (12), the thrust vector angle can be determined as

$$\delta_c = \tan^{-1}\left(\frac{\pm m\sqrt{(V\dot{\chi}_c \cos\gamma)^2 + (V\dot{\gamma}_c + g\cos\gamma)^2}}{m\dot{V}_c + D + mg\sin\gamma}\right) \tag{16}$$

and finally, squaring and adding Eqs. (12) through (14) and taking the square root of the result,

$$T_c = \sqrt{(mV\dot{\chi}_c \cos\gamma)^2 + (mV\dot{\gamma}_c + mg\cos\gamma)^2 + (m\dot{V}_c + D + mg\sin\gamma)^2} \tag{17}$$

Drag— D —in Eqs. (16) and (17) is a function of V and density of air, which is determined based on estimated altitude. The state variables in Eqs. (15) through (17) are estimated quantities. $\dot{V}_c$, $\dot{\chi}_c$ and $\dot{\gamma}_c$ needed in the above equations can be determined by defining control laws for controlling the corresponding state variables. Cruise control for the airspeed to follow the commanded airspeed leads to

$$\dot{V}_c = K_{pv}(V_c - \tilde{V}) \tag{18}$$

where K_{pv} is the proportional gain and $\tilde{V}$ is the estimated airspeed based on measured airspeed. Similarly, a proportional-derivative controller could be employed for generating commands for following the commanded heading angle. With $K_{p\chi}$ as the proportional gain and $K_{d\chi}$ as the derivative gain of the heading controller, and $\tilde{\chi}$ and $\tilde{\dot{\chi}}$ as the estimated heading angle and the heading-angle rate, respectively,

$$\ddot{\chi}_c = K_{p\chi}(\chi_c - \tilde{\chi}) - K_{d\chi}\tilde{\dot{\chi}} \tag{19}$$

In this study, the vertical profile is defined by specifying γ_c in the different phases of flight; it is assumed that the commanded flight-path angle is instantly achieved. Thus, $\tilde{\gamma}$, the estimated flight-path angle, is set equal to γ_c. Furthermore, the commanded flight-path angle rate is set to zero,

$$\dot{\gamma}_c = 0 \tag{20}$$

The commanded angular acceleration in Eq. (19) is integrated forward in time to determine the commanded heading-angle rate for use in Eqs. (15) through (17). Note that limits can be placed on the bank angle and acceleration commands generated by Eq. (15) and Eq. (18), respectively, to accommodate passenger ride quality requirements. Application of proportional control, especially in Eq. (19), can be a bit tricky for large angular differences because of the two ways of turning from one direction to the other—clockwise and counterclockwise, one of which results in a smaller angular rotation; therefore, the smaller angular difference and the direction of the turn needs to be determined.

It is straightforward to specify the airspeed in different phases of flight provided enough thrust can be generated for overcoming the drag, gravitational and wind forces for accelerating the aircraft. Specification of heading and flight-path angle is based on the horizontal and vertical paths to be followed in the presence of wind. This is discussed in the next section.

V. Reference Command Generation

To stay on course in a wind field, the aircraft has to crab such that the across-track component of the wind is cancelled. This assumes that the aircraft has enough speed to counter the wind. The airmass-relative heading angle needed to stay on the path specified by the course angle χ_g is obtained from the two relations based on Fig. 1:

$$V\cos\gamma\cos\chi + W_n = V_g\cos\chi_g \tag{21}$$

and

$$V\cos\gamma\sin\chi + W_e = V_g\sin\chi_g \tag{22}$$

as

$$\chi = \chi_g + \sin^{-1}\left(\frac{W_n\sin\chi_g - W_e\cos\chi_g}{V\cos\gamma}\right) \tag{23}$$

from the trigonometric identity resulting from the difference of Eq. (21) multiplied by $\sin\chi_g$ and Eq. (22) multiplied by $\cos\chi_g$. To compute the desired airmass-relative heading angle using Eq. (23), χ_g has to be specified using a navigation procedure like great-circle navigation to follow the desired route (horizontal path) of flight. The closed-loop great-circle navigation law is given in the following form in Ref. 13:

$$\chi_g = \tan^{-1}\left\{\frac{\sin(\tau_c - \tau)\cos\lambda_c}{\sin\lambda_c\cos\lambda - \cos\lambda_c\sin\lambda\cos(\tau_c - \tau)}\right\} \tag{24}$$

where the current position of the aircraft is (λ, τ) and the commanded position is (λ_c, τ_c) for heading to the next waypoint along the route or directly to the destination. Airmass-relative heading angle command can now be computed using estimated values of latitude and longitude— $\tilde{\lambda}$ and $\tilde{\tau}$ —in Eq. (24), and airspeed and flight-path angle in Eq. (23). Thus,

$$\chi_c = \tilde{\chi}_g + \sin^{-1}\left(\frac{W_n\sin\tilde{\chi}_g - W_e\cos\tilde{\chi}_g}{\tilde{V}\cos\tilde{\gamma}}\right) \tag{25}$$

This commanded heading angle value is used in Eq. (19).

Like the heading angle that needs to be specified for following the horizontal path, flight-path angle needs to be specified for following the vertical path. For example, to maintain level flight in cruise, Eq. (8) prescribes the flight-path angle to be

$$\gamma_c = -\sin^{-1}\left(\frac{W_h}{\tilde{V}}\right) \tag{26}$$

which means that a vertical rate has to be generated to counter vertical wind. The commanded airmass-relative flight-path angle can also be computed for following a climb/descent path prescribed via ground-relative flight-path angle. The ground-relative flight-path angle can be specified as

$$\gamma_g = \tan^{-1}\left(\frac{h_c - h}{d_{GC}}\right) \tag{27}$$

where h_c is the commanded altitude, h is the estimated (current) altitude, and the great-circle distance d_{GC} is

$$d_{GC} = R\cos^{-1}\{\sin\lambda\sin\lambda_c + \cos(\tau_c - \tau)\cos\lambda\cos\lambda_c\} \tag{28}$$

The numerator and denominator in Eq. (27) are altitude-to-go and distance-to-go, respectively. Using Eqs. (8) and (9), the relation between γ and γ_g is

$$\frac{V\sin\gamma + W_h}{\sqrt{(V\cos\gamma\cos\chi + W_n)^2 + (V\cos\gamma\sin\chi + W_e)^2}} = \tan\gamma_g \tag{29}$$

Because the commanded heading angle is available from Eq. (25), commanded airspeed V_c is specified and γ_g is available from Eq. (27), γ —and equivalently γ_c —is the only unknown in Eq. (29). If the vertical component of the wind is ignored, Eq. (29) reduces to a quadratic, which can be easily solved to determine γ_c. Keeping the vertical component of wind results in a quartic equation. Observe that without the wind terms, Eq. (29) simplifies to

$$\gamma_c = \tilde{\gamma}_g \tag{30}$$

γ_c computed via Eq. (29) is assumed to be instantly achieved; it is used directly in Eqs. (15) through (17) for computing the controls.

For vertical descent to the airport/vertiport surface—final descent, γ_g has to be maintained at -90 degrees. This can be accomplished with $V_g = 0$ and a positive descent rate of $-V_h$. The constraint $V_g = 0$ means that both the north and east components of the ground-relative aircraft velocity must be zero. Setting V_{gn} and V_{ge} to zero in Eqs. (6) and (7) results in

$$\tan\chi = \frac{W_e}{W_n} = \tan\chi_w = \tan(\pi + \chi_w) \tag{31}$$

and

$$\cos\gamma = \pm\frac{\sqrt{W_n{}^2 + W_e{}^2}}{V} \tag{32}$$

Equation (31) says the airmass-relative heading angle should be either in the direction of the horizontal component of the wind velocity or opposite to it. See Fig. 1 for a pictorial depiction of the horizontal component of wind velocity. Flying into the wind—opposite direction to the horizontal component of the wind velocity—enables zero groundspeed to be achieved by applying the horizontal component of the airmass-relative velocity in the forward direction. Combining Eq. (32) with Eqs. (8) and (3),

$$\gamma_c = \tan^{-1}\left\{\frac{\dot{h}_c - W_h}{\sqrt{W_n{}^2 + W_e{}^2}}\right\} \tag{33}$$

This commanded flight-path angle can be achieved provided

$$V_c = \sqrt{(\dot{h}_c - W_h)^2 + (W_n{}^2 + W_e{}^2)} \tag{34}$$

The commanded descent rate $\dot{h}_c$ in Eqs. (33) and (34) needs to be specified for landing the aircraft and reducing the descent rate to zero (or close to zero) on touchdown. Starting with a descent rate of $-\dot{h}$ at altitude h, the deceleration required for reducing the descent rate to zero after traversal of distance h is obtained using the kinematic relation between acceleration, initial and final speeds and distance as follows.

$$\ddot{h}_c = \frac{\left(\tilde{\dot{h}}\right)^2}{2\tilde{h}} \tag{35}$$

The feedback control law given by Eq. (35) assumes positive descent rate—$\dot{h}$ has a negative value—and positive h. Because the deceleration required depends on the initial descent rate according to Eq. (35), the initial descent rate needs to be such that the deceleration does not exceed the specified deceleration limit. If the starting altitude for vertical descent for landing is h_{li} and the deceleration limit is $a_{\lim}$, the initial descent rate according to Eq. (35) needs to be

$$\dot{h}_{li} = -\sqrt{2a_{\lim}h_{li}} \tag{36}$$

This completes the description of the variables that need to be specified for computing the controls in all phases of flight.

The trajectory can be determined using either the thrust, thrust vector angle and bank angle—directly as controls—or that resulting from models of thrust, thrust vector angle and bank angle dynamics—driven by the commanded controls—in the equations of motion. The trajectory generation process and an example of the generated trajectory along with the time histories of the control variables are discussed in the next section.

VI. Trajectory Generation

The complete procedure for trajectory generation is summarized in Fig. 3. The process is initiated by reading the flight plan, which provides basic information about the type of aircraft, equipage, origin, destination, route of flight, cruise altitude and cruise speed. Flight plans also specify alternative airports and provide additional information required for operating in the U. S. airspace. The flight procedure (also called airline procedure) describes how the aircraft is to be flown. For example, it might stipulate that after takeoff from the vertiport, the aircraft will climb vertically to 50 feet altitude maintaining a climb rate of 500 feet/minute. It will then climb to the cruise altitude of 2,000 feet while maintaining a 10-degree climb angle and a speed of 60 knots. On reaching the cruise altitude, the aircraft will accelerate to the cruise speed of 98 knots and maintain it, and so on. The next step is to read the initial conditions like the location of the flight, altitude and speed for example.

After reading the required data, the recursive part of the process is begun by determining the mode of flight, where the modes of flight include: on ground, takeoff and initial climb, climb, cruise, initial descent, approach and final descent to landing. These modes are determined as a function of altitude, speed and location of the flight with respect to reference locations such as the origin and destination of flight. Based on the mode of flight, reference commands are generated as shown in Section V using the measured and estimated states, and the desired states needed for tracking the path and speed profiles. The reference commands and the estimated states are then used to determine the controls

as discussed in Section IV. The computed controls are input to the equations of motion, described in Section III, and integrated forward in time to determine the true states. Because the true states of the aircraft are unavailable, a combination of sensors such as Global Positioning System (GPS), accelerometers and gyros are needed along with state estimators running on onboard computers to estimate them. The estimated states are used for onboard control computations for controlling the motion of the physical aircraft. In the ATM systems, observable states are estimated using the aircraft position data acquired by surveillance with radar and transponder-based systems and received from aircraft equipped with an Automatic Dependent Surveillance system. Depending on the degree of realism desired, the "Estimate states" step in Fig. 3 can be as simple as (a) setting the estimated states to the true states, or it can be a bit more complex as (b) adding noise and bias to the true states according to estimation error distributions, or it can be as realistic as (c) modeling the surveillance sensors with their sources of errors and using an Extended Kalman Filter for state estimation. The estimated and the true states are stored for further analysis. The estimated states are then used for determining the mode of flight in the next recursive step. The recursive process is terminated when the mode of flight transitions to "on ground" at the destination. The trajectory consisting of the temporal history of the position—latitude, longitude and altitude—is output in the final step of the trajectory generation process outlined in Fig. 3.

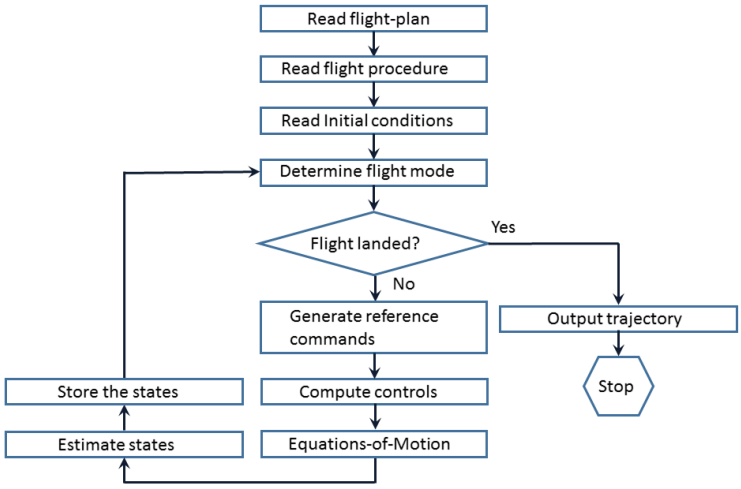

Figure 3. Trajectory generation process.

The procedure summarized in Fig. 3 was utilized for computing the trajectory of the six-passenger multirotor aircraft with takeoff mass of 2,940 kg (see Table 1 for other parameters) flying from Palo Alto Airport (PAO), California to San Martin Airport (E16), California. The two airports are 34 nautical miles apart. PAO is located at 37.46 degrees latitude and -122.11 degrees longitude, and E16 is located at 37.08 degrees latitude and -121.60 degrees longitude. The simulated horizontal trajectory is shown in Fig. 4 and the vertical trajectory is shown in Fig. 5. The

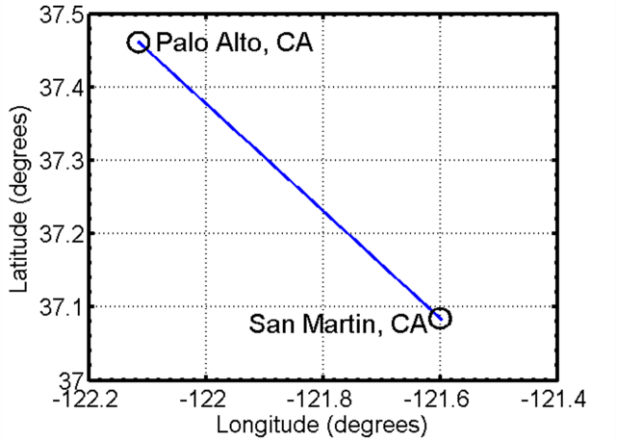

Figure 4. Horizontal trajectory.

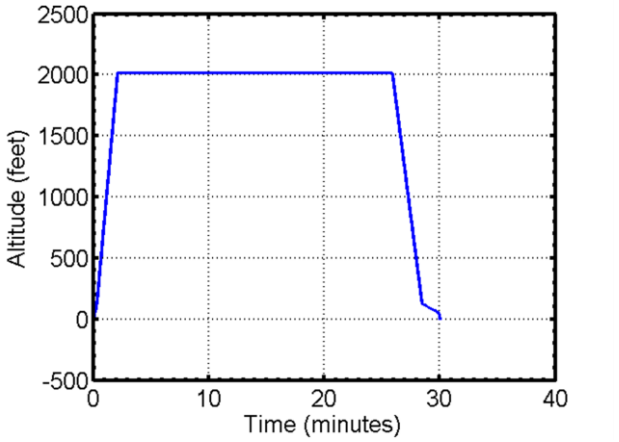

Figure 5. Vertical trajectory.

first four minutes and the last five minutes of flight-path angle time history are shown in Figs. 6a and 6b, respectively. Figure 6a shows the aircraft climbs vertically (90 degrees), climbs at a 10-degree flight-path angle and then levels off for cruise. Figure 6b shows the aircraft initially descends at a -10-degree ground-relative flight-path angle (see Eq. (27)) after the end of cruise. The aircraft then reduces speed to the final descent speed (according to Eqs. (34) and (36)) and descends at a steeper flight-path angle (about -30 degrees) to reduce the descent speed to zero on touchdown

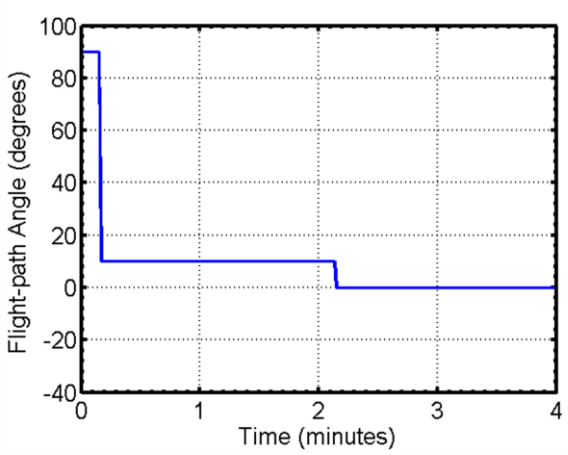

Figure 6a. First four minutes of the flight-path angle time history.

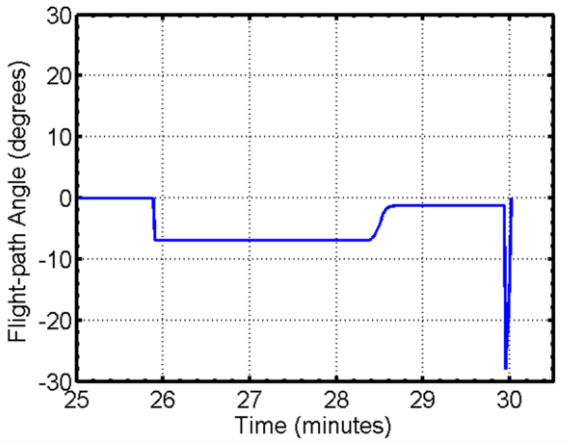

Figure 6b. Last five minutes of the flight-path angle time history.

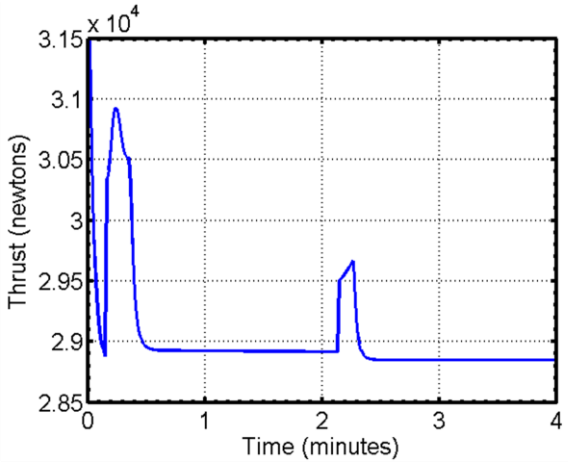

Figure 7a. First four minutes of the thrust time history.

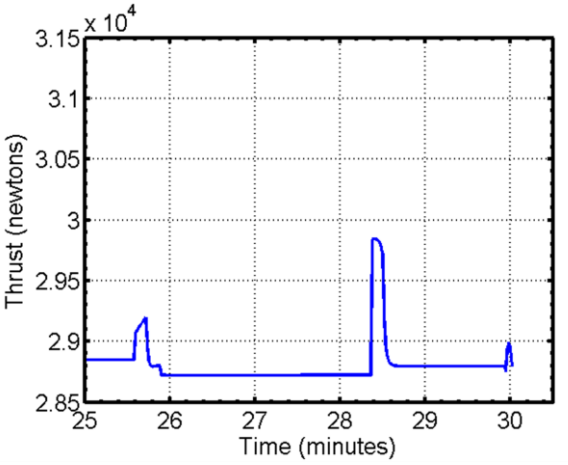

Figure 7b. Last five minutes of the thrust time history.

and to counter the headwind for maintaining groundspeed at zero during vertical descent. The flight-path angle returns to zero as the descent rate is reduced during aircraft descent to the ground. Observe the effect of flight-path angle time history on the vertical trajectory shown in Fig. 5. The thrust required in the different phases of flight: initial vertical climb at 500 feet/minute, 10-degree flight-path angle climb at 60 knots, level off at cruise altitude of 2,000 feet, acceleration from 60 knots to 98 knots (best range speed, Ref. 11) in level flight, deceleration to 60 knots prior to top-of-descent point, -10-degree ground-relative flight-path angle initial descent at 60 knots, slowdown to final descent speed and vertical descent to ground was computed. Figures 7a and 7b show the first four minutes and the last five minutes of the thrust time history. Observe the initial variation in thrust prior to one minute in Fig. 7a. It is due to the bank angle required for reorienting the heading from the initial heading to that required for countering the crosswind component of the wind and heading towards the destination. This figure also shows the increase in thrust between two and three minutes for accelerating from 60 knots to 98 knots in cruise. Figure 7b shows an increase in thrust between 25 and 26 minutes to slowdown from 98 knots to 60 knots, and between 28 and 29 minutes to slowdown from 60 knots to the final descent speed. Figures 8a and 8b show the corresponding first four minutes and the last five minutes of the thrust vector angle w.r.t. horizontal (sum of γ and δ; see Fig. 2) time history. Figure 8a shows the thrust vector angle during initial climb, climb and cruise. Observe the thrust vector angle exceeds 90 degrees between 25 and 26 minutes and between 28 and 29 minutes in Fig. 8b. Angle greater than 90 degrees is for pointing the thrust in the opposite direction of motion to slowdown the aircraft. Figures 9a and 9b show the early and the later parts of the bank

angle time history. The initial bank angle is for turning the aircraft from its initial heading to that required for countering the crosswind and flying towards the destination. Note the correspondence between the bank angle in Fig.

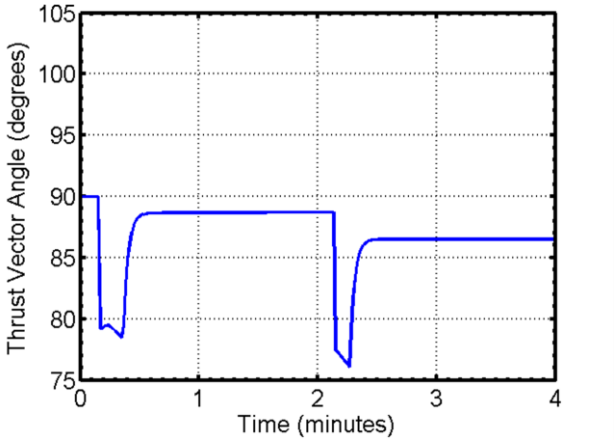

Figure 8a. First four minutes of thrust vector angle time history.

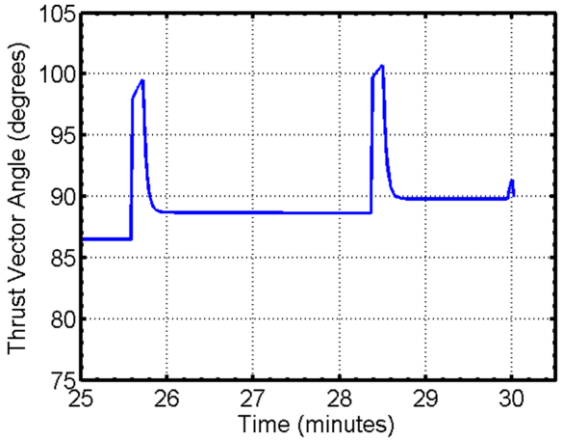

Figure 8b. Last five minutes of the thrust vector angle time history.

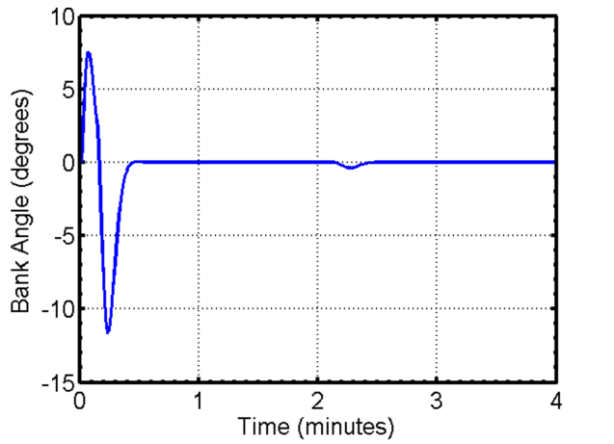

Figure 9a. First four minutes of the bank angle time history.

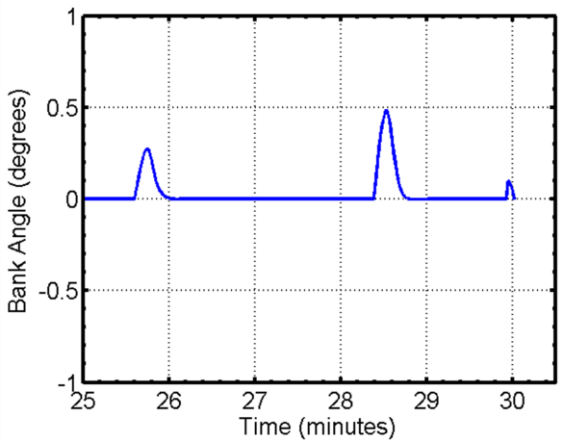

Figure 9b. Last five minutes of the bank angle time history.

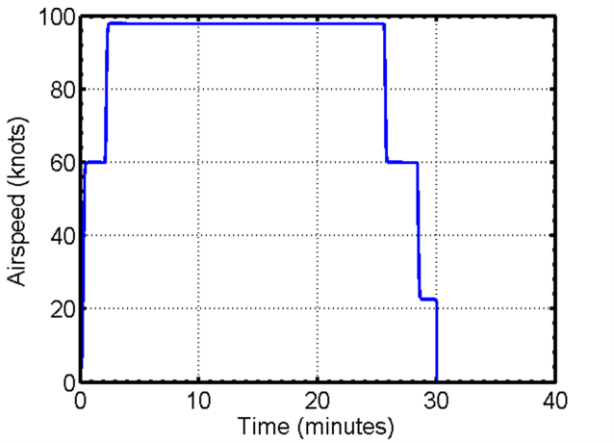

Figure 10. Airspeed time history.

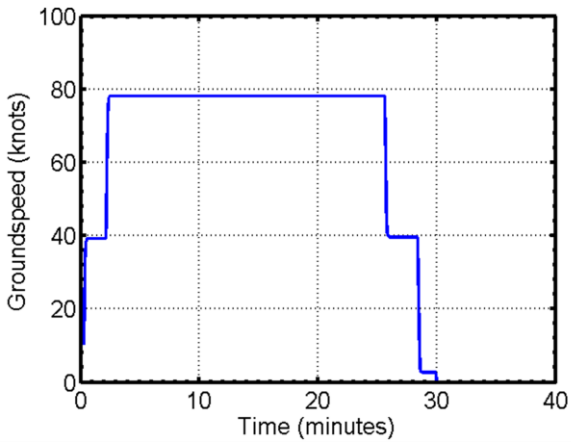

Figure 11. Groundspeed time history.

9a and the thrust prior to one minute in Fig. 7a. Figures 10 and 11 show the airspeed and groundspeed time histories, respectively. Observe in Figs. 10 and 11 that in the approach segment prior to final vertical descent, the airspeed is over 20 knots while the groundspeed is less than three knots against a headwind of 20 knots. The groundspeed is zero during final descent; airspeed is reduced to zero on touchdown.

VII. Conclusions

The results in this paper demonstrate that the performance of the point-mass model of the multirotor electric vertical takeoff and landing aircraft driven by the controllers developed in this paper is suitable for generating trajectories for meeting urban air mobility mission requirements. The ability to generate these trajectories will enable concept evaluation and development of decision support tools for accommodating urban air mobility operations in the air traffic management system.

References

[1]Falck, R. D., Ingraham, D., and Aretskin-Hariton, E., "Multidisciplinary Optimization of Urban-Air-Mobility Class Aircraft Trajectories with Acoustic Constraints," *Proc. AIAA/IEEE Electric Aircraft Technologies Symposium*, Cincinnati, OH, July 9-11, 2018.

[2]Bouadi, H., and Mora-Camino, F., "Modeling and Adaptive Flight Control for Quadrotor Trajectory Tracking," *Journal of Aircraft*, Vol. 55, No. 2, March-April, 2018.

[3]Hoffmann, G. M., Waslander, S. L., and Tomlin, C. J., "Quadrotor Trajectory Tracking Control," *Proc. AIAA Guidance, Navigation, and Control Conference*, Honolulu, HI, August 18-21, 2008.

[4]Hoffmann, G. M., Huang, H., Waslander, S. L., and Tomlin, C. J., "Quadrotor Flight Dynamics and Control: Theory and Experiment," *Proc. AIAA Guidance, Navigation, and Control Conference and Exhibit*, Hilton Head, SC, August 20-23, 2007.

[5]Zawiski, R., and Blachuta, M., "Dynamics and Optimal Control of Quadrotor Platform," *Proc. AIAA Guidance, Navigation, and Control Conference*, Minneapolis, MN, August 13-16, 2012.

[6]Wong, G. L., "The Dynamic Planner: The Sequencer, Scheduler, and Runway Allocator for Air Traffic Control Automation," NASA TM-2000-209586, National Aeronautics and Space Administration, Ames Research Center, Moffett Field, CA 94035-1000, April 2000, URL: http://www.aviationsystemsdivision.arc.nasa.gov/publications/full_list_by_author.shtml [cited: 11/20/2019]

[7]Bilimoria, K., Sridhar, B., Chatterji, G., Sheth, K., and Grabbe, S., "FACET: Future ATM Concepts Evaluation Tool," Air Traffic Control Quarterly, Vol. 9, No. 1, pp. 1-20, 2001,
URL: http://www.aviationsystemsdivision.arc.nasa.gov/publications/full_list_by_author.shtml [cited: 11/20/2019]

[8]Meyn, L., Windhorst, R., Roth, K., Drei, D. V., Kubat, G., Manikonda, V., Roney, S., Hunter, G., Huang, A., and Couluris, G., "Build 4 of the Airspace Concept Evaluation System," *Proc. AIAA Modeling and Simulation Technologies Conference and Exhibit*, Keystone, Colorado, Aug. 21-24, 2006.

[9]"User Manual for Base of Aircraft Data (BADA) Revision 3.6," Eec note no. 10/04, Eurocontrol Experimental Centre, July 2004.

[10]Patterson, M. D., Antcliff, K. R., and Kohlman, L. W., "A Proposed Approach to Studying Urban Air Mobility Missions Including and Initial Exploration of Mission Requirements," *Proc. American Helicopter Society International 74th Annual Forum & Technology Display*, Phoenix, AZ, May 14-17, 2018.

[11]Silva, C., Johnson, W., Antcliff, K. R., and Patterson, M. D., "VTOL Urban Air Mobility Concept Vehicles for Technology Development," *Proc. AIAA Aviation Technology, Integration, and Operations Conference*, Atlanta, GA, June 25-29, 2018.

[12]Chatterji, G. B., "Fuel Burn Estimation Using Real Track Data," AIAA 2011-6881, *Proc. AIAA Aviation Technology, Integration, and Operations Conference*, Virginia Beach, VA, September 20-22, 2011.

[13]Chatterji, G. B., Sridhar, B., and Bilimoria, K. D., "En-route Flight Trajectory Prediction for Conflict Avoidance and Traffic Management," AIAA 96-3766, *Proc. AIAA Guidance, Navigation, and Control Conference*, San Diego, CA, July 29-31, 1996.